nature climate change

SUPPLEMENTARY INFORMATION

DOI: 10.1038/NCLIMATE1449

Multistability and critical thresholds of the Greenland ice sheet

Alexander Robinson[1,2,3], Reinhard Calov[1] & Andrey Ganopolski[1]

February 7, 2012

[1]Potsdam Institute for Climate Impact Research, Potsdam, Germany
[2]Universidad Complutense de Madrid, Madrid, Spain
[3]Instituto de Geociencias (IGEO), CSIC-UCM, Spain

Supplementary Methods

Climatic uncertainty

REMBO uses the ERA-40 climatology [1] over the boundary ocean points to drive the energy-moisture balance model over Greenland. In this study, we applied a spatially constant temperature anomaly to the ERA40 temperature data in all experiments. We prescribed the summer temperature anomaly and we defined the winter anomaly to be twice as large. A sine curve produced the seasonally-varying temperature anomaly actually seen by REMBO. A temperature anomaly that is twice as strong in winter is consistent with predictions from the CMIP3 AOGCMs [2, 3] (see Fig. S1a). Even higher "winter amplification" could occur, however in the AOGCMs, such values are only seen early in the transient simulations, while they tend to equilibrate towards a factor of 2.0. Since the choice of this value has less of an effect on melting itself and more effect precipitation changes, and in order to limit the computational needs of the ensemble, we chose to keep the winter amplification factor constant at 2.0 and treat precipitation separately. Meanwhile, surface melting in Greenland occurs only during summer, so it is

natural to discuss anomalies in terms of the regional summer anomaly rather than the regional mean temperature. It is also quite useful to understand how this relates to the gobal mean temperature, which we are able to do via regional temperature scaling coefficients.

The climatic uncertainty considered here concerns the conversion of temperatures from regional summer to global mean values and the change in precipitation versus increased temperatures. Recently, Frieler et al. [4] estimated regional scaling coefficients for the temperature and precipitation over Greenland relative to the global mean temperature change. Using decadal averages of the CMIP3 database of AOGCM model simulations under global warming [2], they calculated these coefficients from a two-dimensional linear regression of temperature and precipitation over Greenland relative to the global mean temperature. The results are consistent with previous estimates (eg, for precipitation [5]) and properly account for inter-model, inter-scenario and inter-run uncertainty, as well as the correlation between temperature and precipitation. The scaling coefficients used in this study and shown in Fig. S1 were obtained from a one-dimensional version of the model (not accounting for the correlation between temperature and precipitation), however the distributions compare very well with the two-dimensional version. We were thus able to estimate the AOGCM-predicted scaling of the regional increase in winter temperature per degree of regional summer warming (Fig. S1a), the regional summer warming per degree of global mean warming (Fig. S1b) and the regional increase in precipitation per degree of regional summer warming (Fig. S1c).

Under different global warming scenarios, it can be seen that the summer warming around Greenland will be close to the global mean with a narrow spread (with a ratio of $0.9 \pm 0.2\,^{\circ}\mathrm{C}/^{\circ}\mathrm{C}$, Fig. S1b). In fact, this ratio could be slightly different in equilibrium, due to the large thermal inertia of the North Atlantic. Nonetheless, as these transient simulations are the only ones available, we take the probability distribution shown in Fig. S1b to be representative of this ratio in equilibrium and apply it to determine the global mean temperature of the threshold for decline of the Greenland Ice Sheet (GIS), as explained below.

The AOGCMs also estimate an increase in precipitation of $6.3 \pm 3.3\,\%/^{\circ}\mathrm{C}$ with respect to summer warming over Greenland (Fig. S1c). This range of uncertainty can change the surface mass balance of the ice sheet considerably and with it, the threshold for its decline. We therefore chose 9 model versions that evenly cover the most likely range of the AOGCM model spread, from

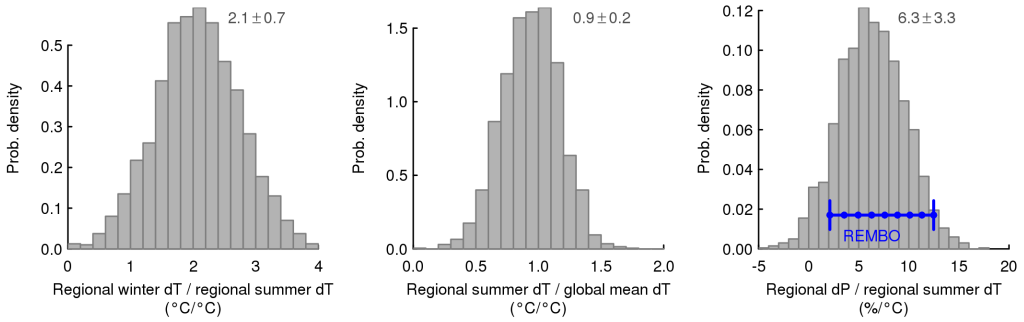

Figure S1: **Probability distributions of scaling coefficients from AOGCMs**. (a) Ratio of the regional winter warming to the regional summer warming, (b) ratio of the regional summer warming to the global mean warming and (c) the perecent increase in precipitation per degree of regional summer warming. All distributions were obtained from a one-dimensional version of the analysis by Frieler et al. [4]. The blue points show individual REMBO model version values and the blue line shows the total REMBO range.

2-12 %/°C (Fig. S1c).

Probability distributions

The curves in Fig. S3 (see below "Individual stability curves") represent the prior (unweighted) ensemble of simulations used to derive the regional temperature thresholds. At this stage, each ensemble member has equal weight and is entirely determined by the choice of the c parameter from the melt equation and the regional precipitation scaling level p.

Next we weighted the ensemble members based on the probability distribution of parameter c and the precipitation scaling p. Each value of parameter c was given equal weight (i.e., a flat distribution), reflecting the large uncertainty of this parameter. We assumed that the distribution of p, shown in Fig. S1c, can be represented by a Gaussian distribution ($6.3 \pm 3.3\,\%/°\mathrm{C}$). The probability of the regional temperature threshold T_{reg} estimated by each combination of c and p was therefore calculated as:

$$P(T_{\mathrm{reg},i,j}) = P(c_i)\,P(p_j) \tag{S1}$$

To calculate a probability distribution from this discrete set of samples, we approximated the empirical cumulative distribution function with a smooth spline and then took the derivative. The resulting distributions of the regional temperature threshold are shown in Fig. 2. The best estimate for the regional summer temperature threshold is 1.8 °C. This estimate is quite robust with respect to the choice of the prior probability distribution for both the c parameter and scaling p (e.g., assuming a normal prior distribution instead of a flat distribution and vice-versa).

To convert the threshold estimates from regional summer temperatures T_{reg} into global mean temperatures T_{glob}, we divided each regional value by discrete values of the scaling factor f, sampled evenly from the AOGCM-estimated distribution shown in Fig. S1b (again assumed to be represented by a Gaussian distribution: 0.9±0.2 °C/°C). By assuming probabilistic independence of the factor f and the other parameters c and p, it was possible to calculate the probability of the global temperature threshold T_{glob} estimated by each combination of c, p and f as:

$$P(T_{\mathrm{glob},i,j,k}) = P(c_i)\,P(p_j)\,P(f_k) \tag{S2}$$

The probability distribution was again calculated by smoothing the empirical cumulative distribution function and taking the derivative. The distributions of the global mean temperature thresholds are shown in Fig. 2b, and a table summarizing the important distribution values are shown in Table S1.

Table S1: Best estimates and credible intervals for the critical temperature thresholds of the GIS (°C), both for the regional summer and the global mean temperature anomaly relative to preindustrial. The upper section shows thresholds for decline of the GIS and the last line shows the threshold for growth of the ice sheet.

	Best	66%	95%
Coupled model (regional summer)	1.8	1.3 - 2.0	1.1 - 2.3
Negative SMB (regional summer)	2.7	2.3 - 3.1	2.0 - 3.5
Coupled model (global mean)	1.6	1.2 - 2.2	0.8 - 3.2
Negative SMB (global mean)	2.6	2.0 - 3.5	1.6 - 4.8
Coupled model (regional summer)	0.4	0.0 - 0.7	-0.2 - 1.0

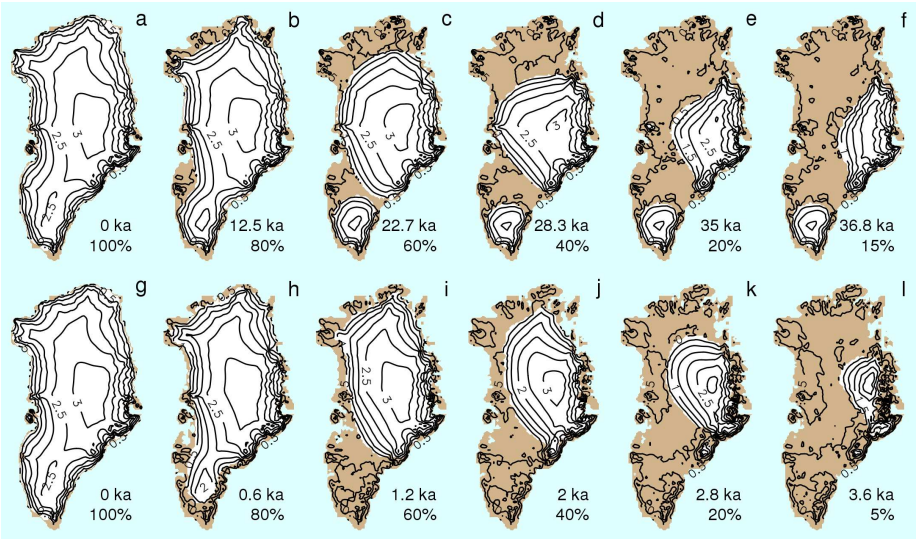

Figure S2: Snapshots of GIS corresponding to different volumes obtained in transient experiments with applied constant temperature anomalies of 2 °C (a-f) and 6 °C (g-l). Note the different time scales of decline for each case. The last column shows the minimum volume distribution reached in each case.

Supplementary Discussion

Transient decline of the GIS

In Fig. S2, the transient evolution of the ice sheet is shown for the case of 2 °C of warming (upper row) and 6 °C of warming (lower row), for the representative model version. Significant differences can be seen between these two cases, both in the time scale of melt and the ice distribution. The latter (6 °C warming case) can be compared to simulations by Ridley et al. [6] (Fig. 5 of their paper), performed with an AOGCM coupled to an ice sheet model in a climate with four times CO_2 (6 °C of warming corresponds to approximately four times CO_2, assuming a climate sensitivity of 3 °C). Our simulations show a very similar pattern of melt (panels g-l) with the southwestern part of the ice sheet disappearing first and finally retreating to the high elevation eastern region. The time scale of melt is also comparable, although here complete melting of the GIS requires several hundred years

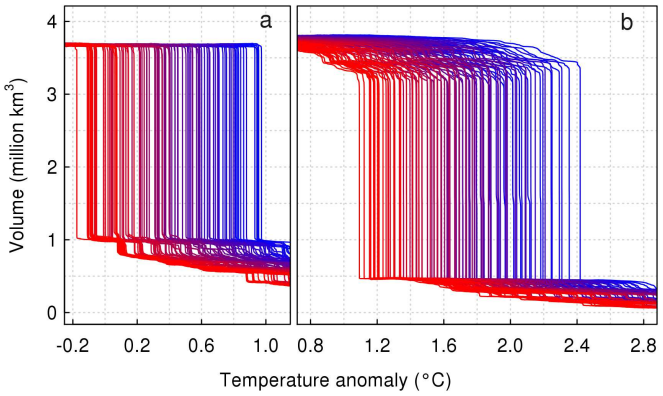

Figure S3: (a,b) Individual stability curves of the GIS as functions of the regional summer temperature anomaly, focused on growth and decline of the ice sheet, respectively, for all 99 simulations in the ensemble. The color shading from red to blue indicates the value of parameter c used for each simulation (from -50 to -60 W/m^2).

more compared to the coupled AOGCM simulation [6], which likely at least partly results from the lack of additional warming over the ocean in our simulations that could increase melt rates in a fully coupled model.

Melting of the GIS under 2 °C of warming (Fig. S2a-f) shows a different pattern and time scale. Since this temperature is close to the threshold temperature, the ice sheet needs approximately 50,000 years to melt completely. On this time scale, competing processes, such as bedrock uplift and ice flow adjust the distribution of the ice to maintain quasi-equilibrium with the climate. Thus, in this case, the northern part of the ice sheet also becomes quite sensitive to warming, since this region has the lowest accumulation rates. In model versions with high precipitation increases, the southern portion of the ice sheet actually melts much later than in the North, since most of the precipitation comes to the South. For the higher temperature anomaly of 6 °C, a strong increase in melt rates in the South cause it to lose mass the fastest, but in any case, the entire ice sheet disappears in less than 4000 years.

Individual stability curves

Figure S3 shows the individual results from the quasi-equilibrium experiments for the stability of the GIS under climate change. The largest uncertainty comes from the choice of the melt model parameter c, as reflected by the color progression in the figure, while uncertainty in precipitation plays a secondary role. The evolution of the quasi-equilibrium GIS states along upper and lower branches for the representative model version is illustrated by the animations included with Supplementary Information.

Simulations of the basins of attraction

The approach presented previously by Ridley et al. [7] was used as the basis for our simulations of GIS regrowth after partial loss of volume and area. The question addressed here is: when a portion of the GIS has melted away and the boundary temperature is returned to a lower value (e.g., by eventually reducing the atmospheric CO_2 concentration), will the ice sheet regrow, find a new equilibrium or continue to decline irreversibly? These simulations were performed for the representative model version (as in Fig. 1). The climate and surface mass balance fields were updated every 10 years to account for feedbacks and changes in the ice sheet topography. To obtain the initial reduced-volume ice sheet configurations, the present-day GIS resulting from a paleo simulation [8] was prescribed as the initial ice sheet, and an instantaneous, constant temperature anomaly of 1.8 °C was applied. As the ice sheet lost volume, the simulated ice sheet state was saved at intervals of 5% of volume loss (several states are similar to those shown in Fig. S2a-f). In this way, 17 different ice sheet configurations were produced, which were then used as initial conditions to determine the domains of attractions of different equilibrium branches of the hysteresis curve.

The fractional states ranging from 15-95% were used to test how different temperature anomalies (in and near the multi-stable region) applied to a reduced-volume ice sheet would affect the final equilibrium state. Ridley et al. [7] tested only one case, with the temperature anomaly equal to 0.0 °C (preindustrial conditions). We extended this experiment by testing several temperatures in and near the multi-stable region of the stability diagram (at intervals of 0.1 °C). Every simulation was allowed to run for at least 200 ka to ensure equilibrium was reached. This is especially important for temperatures near the bifurcation point, where the time scale for changes is

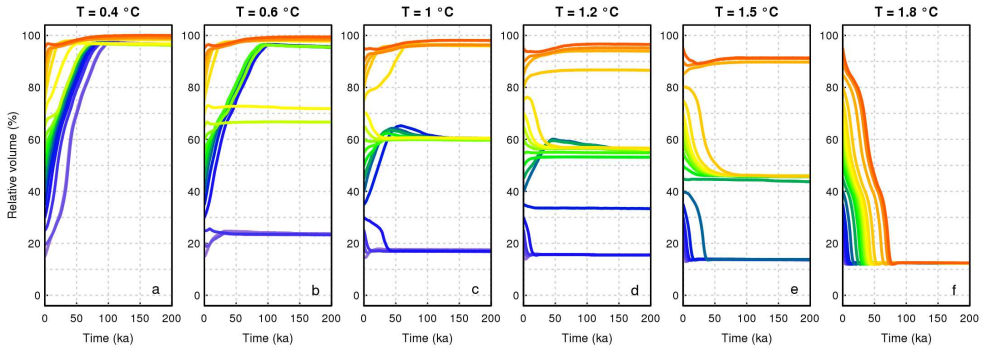

Figure S4: Temporal evolution of ice sheet volume for different temperature anomalies (shown at the top of each panel) and different initial volumes. Each color corresponds to a different initial volume (relative to the present-day state), from 95% (red) to 15% (purple), and a gradually varying colour spectrum between.

extremely slow [9]. Figure S4 shows the transient volume for several cases, with each panel corresponding to a different temperature anomaly. Outside of the multi-stable region, the simulations produce the expected results – for temperature anomalies below the threshold for regrowth (panel a), all simulations regrew to the "full volume" state and for temperature anomalies above the threshold for decay, all simulations result in almost complete melting of the ice sheet (i.e., less than 20% remaining, panel f). Between these two limits, intermediate equilibrium states can exist, and these depend on the temperature anomaly applied (panels b-e). Our simulations corroborate previous results [7] rather well, although new and systematic responses are also revealed from testing multiple temperature anomalies. We find an intermediate equilibrium branch (with ca. 40-60% of the present-day ice volume) that can be traced in a similar way as the upper and lower branches. For lower temperature anomalies, e.g. 1 °C, the intermediate equilibrium state has about 60% of the present-day ice volume. As the temperature increases, this state reduces in volume until about 40% at 1.6 °C, after which this state also collapses to the ice-free equilibrium state.

Figure S5 provides additional information to Fig. 1. Here the final equilibrium states of all reduced-volume runs are also plotted as crosses. The minor differences that can be seen between several equilibrium states and the con-

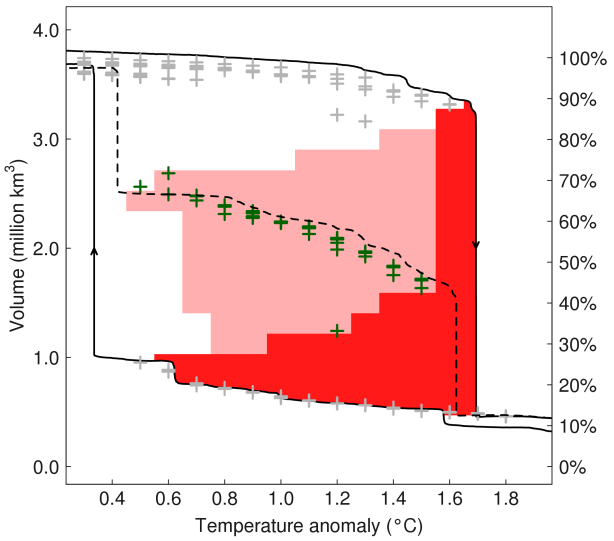

Figure S5: Basins of attraction for the medium sensitivity model shown in Fig. 1, along with the locations of the discrete equilibrium states (grey and green crosses) obtained by long-term simulations for different temperature anomalies and different initial conditions. Grey crosses correspond to equilibrium states that are close to the main branches obtained by continuous tracing of the stability diagram. Green crosses correspond to the intermediate equilibrium states and the dashed line shows the approximate intermediate branch of the stability diagram.

tinuous quasi-equilibrium solution are explained by a relatively coarse spatial resolution of the model. This is the same with the intermediate branch that is higher than most of the intermediate crosses (dashed line). The intermediate branch was obtained by starting from the intermediate equilibrium point for a temperature anomaly of 0.6 °C. Then, as with the upper and lower branches, the temperature was slowly increased and decreased to trace the intermediate branch. The resulting quasi-equilibrium stability branch is more accurate than the individual points, but it is essentially the same result. One resulting intermediate equilibrium point lies away from the others (green cross alone in the pink region). This appears to be a model dependent result and is likely an artifact of the numerical resolution, since it is not as robustly represented as the other locations. Nonetheless, it cannot be ruled out that more than one intermediate branch may exist.

Simulations that start with a large volume fraction for low temperature anomalies (white region of Fig. S5) equilibrate to the upper branch of the stability diagram. Figure 4 in the main text shows an example of this equilibrium state for 1 °C (labelled E1), which is representative of the state of the present-day ice sheet (i.e., fully ice-covered Greenland). Conversely, simulations that start with a very low volume for a high temperature anomaly eventually equilibrate to the lower branch of the stability diagram at around 20% volume fraction, as found by others [7]. Depending on the temperature anomaly, the lower branch varies between volumes of 15-20%, yet we would still consider these cases as representing one equilibrium state, because the distribution of ice is quite similar in each case (see the included animations). As a representative example of this state, Fig. 4 shows the equilibrium ice distribution for the case that started with 15% volume for an applied anomaly of 1 °C (labelled E3). It consists of ice limited to the high elevation mountainous regions in the Southeast, and a small ice cap in the South.

An intermediate state is also found, with a volume of approximately 40-60% of the present-day volume (Fig. 4, labelled E2). This state exists for temperature anomalies in the range of 0.4-1.6 °C. In this case, the ice sheet occupies the southern regions of Greenland and the northern regions remain ice free. This occurs because after melting large portions in the North, lower albedo and low precipitation prevents regrowth of ice in these areas. If the temperature anomaly increases above 1.6 °C, the intermediate ice sheet reaches an unsustainable condition and collapses to the lower branch of the stability diagram.

The three equilibrium states found in this study do not necessarily reflect all possible equilibria. For example, although the intermediate state (E2) is qualitatively rather similar to that found by Ridley et al. [7], it is not identical. Nonetheless, this study demonstrates that for the underlying complex Greenland topography, intermediate states are possible within a certain range of temperature anomalies. Moreover, our stability analysis show that for higher temperature anomalies, less of the ice sheet needs to be melted before the decline becomes irreversible (e.g., for a temperature anomaly of 1 °C, the decline is irreversible after 70% of the ice sheet melts, whereas for an anomaly of 1.6 °C, the decline is irreversible after only 10% of the ice sheet melts).

References

[1] Uppala, S. M. *et al.* The ERA-40 re-analysis. *Q.J.R. Meteorol. Soc.* **131**, 2961–3012 (2005).

[2] Meehl, G. A. *et al.* THE WCRP CMIP3 Multimodel Dataset: A New Era in Climate Change Research. *Bulletin of the American Meteorological Society* **88**, 1383 (2007).

[3] Meehl, G. A. *et al. Climate Change 2007: The Physical Science Basis. Contribution of Working Group I to the Fourth Assessment Report of the Intergovernmental Panel on Climate Change*, chap. Global Cli (Cambridge University Press, Cambridge, UK, 2007).

[4] Frieler, K., Meinshausen, M., Mengel, M., Braun, N. & Hare, W. A scaling approach to probabilistic assessment of regional climate change. *Journal of Climate* 110927043956000 (2011).

[5] Gregory, J. M. & Huybrechts, P. Ice-sheet contributions to future sea-level change. *Philosophical Transactions of the Royal Society A: Mathematical, Physical and Engineering Sciences* **364**, 1709–1732 (2006).

[6] Ridley, J. K., Huybrechts, P., Gregory, J. M. & Lowe, J. A. Elimination of the Greenland Ice Sheet in a High CO_2 Climate. *Journal of Climate* **18**, 3409–3427 (2005).

[7] Ridley, J., Gregory, J. M., Huybrechts, P. & Lowe, J. Thresholds for irreversible decline of the Greenland ice sheet. *Climate Dynamics* **35**, 1049–1057 (2009).

[8] Robinson, A., Calov, R. & Ganopolski, A. Greenland ice sheet model parameters constrained using simulations of the Eemian Interglacial. *Climate of the Past* **7**, 381–396 (2011).

[9] Calov, R., Ganopolski, A., Kubatzki, C. & Claussen, M. Mechanisms and time scales of glacial inception simulated with an Earth system model of intermediate complexity. *Climate of the Past* **5**, 245–258 (2009).